Atmospheric light estimation through vector orthogonality in color degradation space

Lingzhao Kong, Dagang Jiang* , Member, IEEE, Xin Liu, Student Member, IEEE, Yu Zhang

***Abstract*— Atmospheric light estimation is fundamental for image or video dehazing. Unlike previous researches on the atmospheric light estimation, this study reveals a vector orthogonality in the classical atmospheric color degradation model for the first time. It is demonstrated that atmospheric light vector is orthogonal to the normal vectors of color degradation plane. Furthermore, a novel estimation method for direction and magnitude of atmospheric light vector is proposed based on the vector orthogonality. The proposed method can accurately estimate the atmospheric light and improve the quality of image dehazing with a short constant processing time even if the image resolution is increasing. This study provides an efficient approach for estimating atmospheric light for high-definition image or video dehazing applications, such as traffic surveillance, environmental monitoring, and aerial photography.**

***Index Terms*— Atmospheric light, atmospheric scattering model, color vector orthogonality, dehazing**

I. INTRODUCTION

Optical imaging is widely used in applications such as traffic surveillance, environmental monitoring, and aerial photography. Due to the absorption and scattering of atmospheric turbid medium, the optical image goes through degradation in terms of brightness, contrast and color distortion. such a phenomenon is referred to as color degradation. Consequently, the application of optical image is inevitably subject to hazy conditions [1].

The image's color degradation model in the atmosphere is established by McCartney, Narasimhan and Nayar [2-6], which shows that the degraded color consists of two parts: (1) atmospheric light induced additive radiance, and (2) atmospheric transmission (absorption and scattering) induced direct attenuation of the scene radiance. The atmospheric light and atmospheric transmission determine the result of color degradation.

There are two main categories of image dehazing methods: (1) data-driven based methods [7-15] and (2) physical property-based methods [16-32]. In this paper, we focus on the physical property-based methods due to their simplicity and stability.

Most of physical property-based image dehazing methods follow the process described as follows. (1) Estimating the atmospheric light. (2) Estimating the atmospheric transmission based on the atmospheric light estimation. (3) Restoring the haze-free image according the estimation results of atmospheric light and atmospheric transmission.

The atmospheric transmission estimation methods are mainly based on the uncorrelation between the atmospheric transmission and albedo [16], the maximum image block contrast [17], color attenuation prior [18], non-local prior [19], rank-one prior [20], or dark channel prior (DCP) [21]. The DCP have being widely investigated and improved in terms of convenience, fast and stability [25-29].

The main atmospheric light estimation methods are as follows: Tan et al. [1] estimated atmospheric light through the brightest pixels in the image. Tarel et al. [22] estimated atmospheric light as pure-white according to the gray-world assumption. Kim et al. [17] established a quad-tree subdivision (Quad-tree) method to estimate atmospheric light through hierarchical searching. Zhu et al. [18] established a color attenuation prior (CAP) method to estimate atmospheric light based on searching the largest depth area. Sulami and Fattal et al. [16, 23] established an atmospheric light recovery (ATM) method to estimate atmospheric light based on screening the image regions with local smoothness and obtaining spatial

(support information).

This work was supported in part by National Natural Science Foundation of China (No. 61501097), the Chinese F undamental Research Funds for the Central Universities (No. ZYGX2019J080), and the Science & Technology Department of Sichuan Province (No. 2020Z YD016). *Corresponding author:* D. Jiang.

L. Kong is with the School of Astronautics and Aeronautics, University of Electronic Science and Technology of China, Chengdu 611731, China.

D. Jiang is with the School of Astronautics and Aeronautics, University of Electronic Science and Technology of China, Chengdu 611731, China, and also with the Aircraft Swarm Intelligent Sensing and Cooperative Control Key Laboratory of Sichuan Province, Chengdu, Sichuan 611731, China (e-mail: jiangdagang@uestc.edu.cn).

X. Liu is with the School of Astronautics and Aeronautics, University of Electronic Science and Technology of China, Chengdu 611731, China.

Y. Zhang is with the School of Astronautics and Aeronautics, University of Electronic Science and Technology of China, Chengdu 611731, China.

Color versions of one or more of the figures in this article are available online at http://ieeexplore.ieee.org

straight lines with principal component analysis. Berman et al. [31] established a non-local haze-lines (Haze-lines) method to estimate atmospheric light using the Hough transform in RGB space to vote for the atmospheric light. According to the He's suggestions in DCP [21], many studies [18-19, 21, 25-30, 32] estimate atmospheric light by selecting the top 0.1% of the brightest pixels in the dark channel map, which is widely used in the imaging or video systems.

Unlike previous researches on the atmospheric light estimation, we reveal the vector orthogonality in the classical atmospheric color degradation model in this work. Furthermore, we propose a novel atmospheric light estimation method based on the vector orthogonality. Combined with the widely used DCP for atmospheric transmission estimation, a better image or video dehazing result is achieved with accurate atmospheric light estimation. Our contributions can improve the accuracy of atmospheric light estimation for image or video dehazing and improve the running time in the high-definition image or video.

The rest of this paper is organized as follows. In Section II, the related work of atmospheric color degradation model and the DCP dehazing method. In Section III, the vector orthogonality and atmospheric light estimation are deduced. In Section IV, the experimental results are illustrated and compared with five atmospheric light estimation methods (DCP, Quad-tree, CAP, ATM, and Haze-lines). In Section V, the conclusions of this research are summarized.

II. Related Work

A. Atmospheric Color Degradation Model

The atmospheric color degradation model is widely used and expressed in [2]-[6]:

$$\mathbf{I}(\mathbf{x}) = t(\mathbf{x}) \cdot \mathbf{J}(\mathbf{x}) + \left(1 - t(\mathbf{x})\right) \cdot \mathbf{A} \tag{1}$$

where $\mathbf{x}$ is pixel coordinate, $\mathbf{I}(\mathbf{x})$ is the observed image, $t(\mathbf{x})$ is the atmospheric transmission, $\mathbf{J}(\mathbf{x})$ is the scene radiance without atmosphere, and $\mathbf{A}$ is the atmospheric light. $t(\mathbf{x})$ can be further expressed as $t(\mathbf{x}) = e^{-\beta d(\mathbf{x})}$, where β is the atmospheric extinction coefficient and $d(\mathbf{x})$ is the scene depth at $\mathbf{x}$.

B. Dark Channel Prior for Image Dehazing

The dark channel prior [21] considers that at least one-color channel has very low intensity at some pixels in most of the non-sky patches. The atmospheric light $\hat{\mathbf{A}}$ can be estimated through the top 0.1% brightest pixels in the dark channel. Then, the atmospheric transmission can be estimated as:

$$\tilde{t}(\mathbf{x}) = 1 - \omega \cdot \min_{y \in \Omega(x)} \left(\min_{c \in (R,G,B)} \frac{I_c(\mathbf{y})}{\hat{A}_c} \right) \tag{2}$$

where $\Omega(\mathbf{x})$ is a local patch centered at $\mathbf{x}$. $\mathbf{y}$ is pixel coordinate in $\Omega(\mathbf{x})$. c represents one of the RGB channels. $I_c(\mathbf{y})$ is observed image on one channel. $\hat{A}_c$ is one channel value of $\hat{\mathbf{A}}$. The value of ω is application based, which is usually set as 0.95.

The haze-free image can be obtained by combining the Eq. (1)- (2) as follows:

$$\mathbf{J}(\mathbf{x}) = \frac{\mathbf{I}(\mathbf{x}) - \hat{\mathbf{A}}}{\max\left(\tilde{t}(\mathbf{x}),\ t_0\right)} + \hat{\mathbf{A}} \tag{3}$$

where t_0 is the lower bound of transmission $t(\mathbf{x})$.

Evidently, the accuracy of atmospheric light estimation is fundamental for the atmospheric transmission estimation and determines the results of dehazing. In the following parts, we will adopt a new method to estimate atmospheric light, and still use (2) and (3) for image dehazing.

III. Atmospheric Light Estimation Through Vector Orthogonality

A. Vector Orthogonality in Color Degradation Space

Equation (1) can be rewritten as a form of color vector in RGB color degradation space [5]:

$$\begin{aligned} \mathbf{I}(\mathbf{x},d) &= e^{-\beta d} \cdot \mathbf{J}(\mathbf{x}) + \left(1 - e^{-\beta d}\right) \cdot \mathbf{A} \\ &= e^{-\beta d} \cdot \begin{pmatrix} R_J \\ G_J \\ B_J \end{pmatrix} + \left(1 - e^{-\beta d}\right) \cdot \begin{pmatrix} R_A \\ G_A \\ B_A \end{pmatrix} \end{aligned} \tag{4}$$

where $\mathbf{I}(\mathbf{x},d)$ is the color vector of the image in atmosphere. $\mathbf{x}$ and d also represent image coordinate and scene depth, respectively. $\mathbf{J}(\mathbf{x})$ is the color vector of the image without atmosphere and $\mathbf{A}$ is the atmospheric light vector, they are independent of d. The color vector of $\mathbf{J}(\mathbf{x})$ is defined as $(R_J, G_J, B_J)^T$, the color vector of $\mathbf{A}$ is defined as $(R_A, G_A, B_A)^T$.

The relationship of $\mathbf{I}(\mathbf{x},d)$, $\mathbf{J}(\mathbf{x})$, and $\mathbf{A}$ is shown in Fig.1. According to (4), we find that the vectors $\left[\mathbf{A} - \mathbf{I}(\mathbf{x},d)\right]$ and $\left[\mathbf{I}(\mathbf{x},d) - \mathbf{J}(\mathbf{x})\right]$ can be written as:

$$\begin{cases} \mathbf{A} - \mathbf{I}(\mathbf{x},d) = e^{-\beta d} \cdot \left(\mathbf{A} - \mathbf{J}(\mathbf{x})\right) \\ \mathbf{I}(\mathbf{x},d) - \mathbf{J}(\mathbf{x}) = \left(1 - e^{-\beta d}\right) \cdot \left(\mathbf{A} - \mathbf{J}(\mathbf{x})\right) \end{cases} \tag{5}$$

Equation (5) shows that the vectors $\left[\mathbf{A} - \mathbf{I}(\mathbf{x},d)\right]$ and $\left[\mathbf{I}(\mathbf{x},d) - \mathbf{J}(\mathbf{x})\right]$ are colinear, because they have the same direction and vector end point $\mathbf{I}(\mathbf{x},d)$. According to (5), if a color block at $\mathbf{I}(\mathbf{x},d)$ can be moved towards camera (denoted as $\mathbf{I}(\mathbf{x},d^-)$) or away from the camera (denoted as $\mathbf{I}(\mathbf{x},d^+)$), the end points of vectors $\mathbf{I}(\mathbf{x},d)$, $\mathbf{I}(\mathbf{x},d^-)$, and $\mathbf{I}(\mathbf{x},d^+)$ are on the line of $\mathbf{A}$ to $\mathbf{J}(\mathbf{x})$. Equation (5) also shows that,

$\mathbf{I}(\mathbf{x},d)\approx\mathbf{J}(\mathbf{x})$ when d tends to 0, and $\mathbf{I}(\mathbf{x},d)\approx\mathbf{A}$ when d tends to ∞.

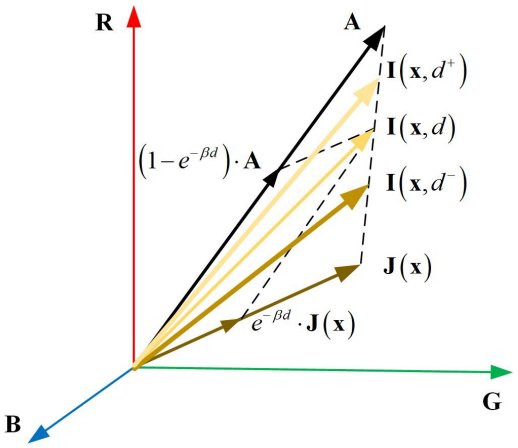

Fig. 1. Relationship of $\mathbf{I}(\mathbf{x},d)$, $\mathbf{J}(\mathbf{x})$, and $\mathbf{A}$

Based on the color vector colinear relationship from (5) it can be inferred that a plane $P_1(\mathbf{x}_1)$ with a particular type of color (denoted as color degradation plane) can be formed by $\mathbf{J}_1(\mathbf{x}_1)$ and $\mathbf{A}$ (see Fig.2). The subscript under P and $\mathbf{J}$ represents different color. The subscript under $\mathbf{x}$ represents different image coordinate. If this type of color block moves at different scene depth d and Δd, the normal vector $\mathbf{n}_1(\mathbf{x}_1)$ of the plane $P_1(\mathbf{x}_1)$ can be obtained as $\mathbf{I}_1(\mathbf{x}_1,d)\times\mathbf{I}_1(\mathbf{x}_1,\Delta d)/\left\|\mathbf{I}_1(\mathbf{x}_1,d)\times\mathbf{I}_1(\mathbf{x}_1,\Delta d)\right\|$. $\|\ \|$ represents the vector module. Similarly, the normal vector $\mathbf{n}_2(\mathbf{x}_2)$ of the plane $P_2(\mathbf{x}_2)$ with different color can also be obtained as $\mathbf{I}_2(\mathbf{x}_2,d)\times\mathbf{I}(\mathbf{x}_2,\Delta d)/\left\|\mathbf{I}_2(\mathbf{x}_2,d)\times\mathbf{I}_2(\mathbf{x}_2,\Delta d)\right\|$.

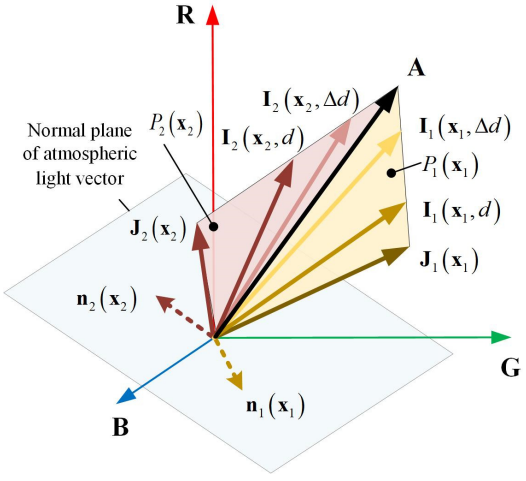

Fig. 2. Vector orthogonality in color degradation plane

From the above, we reveal a new vector orthogonality in the classical atmospheric color degradation model, which is the atmospheric light vector orthogonal to the normal vectors of color degradation plane. $\mathbf{n}_1(\mathbf{x}_1)$ and $\mathbf{n}_2(\mathbf{x}_2)$ are in the normal plane of atmospheric light vector $\mathbf{A}$.

Therefore, the norm direction vector of atmospheric light vector $\mathbf{e}_A$ can be theoretically solved from:

$$\begin{aligned}\left[\mathbf{I}_1(\mathbf{x}_1,d)\times\mathbf{I}_1(\mathbf{x}_1,\Delta d)\right]\cdot\mathbf{e}_A=0\\ \left[\mathbf{I}_2(\mathbf{x}_2,d)\times\mathbf{I}_2(\mathbf{x}_2,\Delta d)\right]\cdot\mathbf{e}_A=0\end{aligned}\tag{6}$$

Because $\left[\mathbf{A}-\mathbf{I}_i(\mathbf{x}_i,d)\right]$ is parallel to $\left[\mathbf{I}_i(\mathbf{x}_i,\Delta d)-\mathbf{I}_i(\mathbf{x}_i,d)\right]$ and $\left[\mathbf{A}-\mathbf{I}_i(\mathbf{x}_i,d)\right]\times\left[\mathbf{I}_i(\mathbf{x}_i,\Delta d)-\mathbf{I}_i(\mathbf{x}_i,d)\right]=\mathbf{0}$, the module of atmospheric light vector $\|\mathbf{A}\|$ can be theoretically calculated as:

$$\|\mathbf{A}\|=\frac{\left\|\mathbf{I}_i(\mathbf{x}_i,d)\times\left[\mathbf{I}_i(\mathbf{x}_i,\Delta d)-\mathbf{I}_i(\mathbf{x}_i,d)\right]\right\|}{\left\|\mathbf{e}_A\times\left[\mathbf{I}_i(\mathbf{x}_i,\Delta d)-\mathbf{I}_i(\mathbf{x}_i,d)\right]\right\|}\tag{7}$$

B. Atmospheric Light Estimation through Vector Orthogonality in a Single Image

Equations (6) and (7) present an ideal approach of estimating atmospheric light vector through the same color blocks moving at two different scene depths, which is difficult to be used in a single image without any actively moving color blocks.

The vector orthogonality in the similar color block could be used for atmospheric light estimation because similar color blocks in a single image can be extracted by clustering algorithm and the small changes of scene depth are implied in the similar color blocks.

In case of using the clustering algorithm to divide the colors into K classes, similar colors in a class could appear at different image coordinate and the scene depth becomes unknown. In addition, various error sources, such as small changes in scene depth, non-uniform atmospheric extinction coefficient, and pixel read-out noise, have been induced in the actual imaging process. They slightly change the image color vector. Therefore, the actual color vector at image coordinate $\mathbf{x}_i$ should be rewritten as $\hat{\mathbf{I}}_k(\mathbf{x}_i)$, where the subscript k ($k=1,2,3\cdots K$) denotes the k th color class, the subscript i ($i=1,2,3\cdots M_k$) denotes the number of pixel in the k th color class.

Because the actual color vector contains imaging and clustering errors, it is inaccurate to estimate the direction of atmospheric light vector $\mathbf{e}_A$ through (6) with only two normal vectors of color degradation planes. However, $\mathbf{e}_A$ is orthogonal to all the normal vectors of color degradation planes, and the normal vector of the k th color degradation plane can be estimated by two different randomly chosen color vectors $\hat{\mathbf{I}}_k(\mathbf{x}_i)$ and $\hat{\mathbf{I}}_k(\mathbf{y}_i)$ in the k th color class. Therefore, $\mathbf{e}_A$ can be estimated by solving the least square solution in the following equations.

$$\min\left\{\sum_{k=1}^{K}\sum_{i=1}^{N_k}\left\{\left[\hat{\mathbf{I}}_k(\mathbf{x}_i)\times\hat{\mathbf{I}}_k(\mathbf{y}_i)\right]\cdot\mathbf{e}_A\right\}\right\}=0 \quad \text{s.t. } \|\mathbf{e}_A\|=1, N_k\le M_k, \hat{\mathbf{I}}_k(\mathbf{x}_i)\neq\hat{\mathbf{I}}_k(\mathbf{y}_i) \tag{8}$$

Fig.3 illustrates the results of $\mathbf{e}_A$ estimated through the normal vectors $\mathbf{n}_i$ from different color degeneration planes.

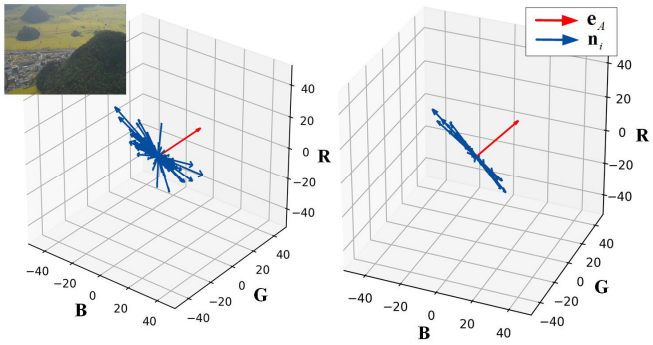

Fig. 3. Illustration of $\mathbf{e}_A$ estimated through the normal vectors $\mathbf{n}_i$ from different color degeneration planes

It is also inaccurate to estimate the module of atmospheric light vector $\mathbf{e}_A$ through (7) with two color vectors in the k th color class, even if the $\mathbf{e}_A$ is obtained by (8). However, the statistical characteristics of $\|\mathbf{A}_i\|$, which is calculated by randomly chosen color vectors $\hat{\mathbf{I}}_k(\mathbf{x}_i)$ and $\hat{\mathbf{I}}_k(\mathbf{y}_i)$ in the k th color class, can be used for accurately estimating $\mathbf{A}$.

As shown in left part of Fig. 4, a color degradation plane $P(\mathbf{x})$ is formed by a randomly chosen color vector $\hat{\mathbf{I}}_k(\mathbf{x})$ and $\mathbf{A}$. $\hat{\mathbf{I}}_k(\mathbf{x})$ can be rewritten as $\mathbf{I}(\mathbf{x})$ due to it can be considered as error free in the $P(\mathbf{x})$. Thus, the other color vectors $\hat{\mathbf{I}}_k(\mathbf{y}_i)$ are outside $P(\mathbf{x})$ due to the imaging and clustering error.

Because $\mathbf{e}_A$ is determined by (8), the normal vector $\mathbf{n}_P$ of $P(\mathbf{x})$ can be obtained through $\mathbf{I}(\mathbf{x})\times\mathbf{e}_A$. Let $\hat{\mathbf{I}}_k(\mathbf{y}_i)=\mathbf{I}_P(\mathbf{y}_i)+\mathbf{r}_{\perp i}$, where $\mathbf{I}_P(\mathbf{y}_i)$ belongs to the $P(\mathbf{x})$, $\mathbf{r}_{\perp i}$ are perpendicular to $P(\mathbf{x})$. Then the $\mathbf{I}_P(\mathbf{y}_i)$ can be solved as:

$$\begin{aligned}\mathbf{I}_p(\mathbf{y}_i)&=\hat{\mathbf{I}}_k(\mathbf{y}_i)-\mathbf{r}_{\perp i}\\&=\hat{\mathbf{I}}_k(\mathbf{y}_i)-\left[\hat{\mathbf{I}}_k(\mathbf{y}_i)\cdot\left[\mathbf{I}(\mathbf{x})\times\mathbf{e}_A\right]\right]\cdot\frac{\left[\mathbf{I}(\mathbf{x})\times\mathbf{e}_A\right]}{\left\|\mathbf{I}(\mathbf{x})\times\mathbf{e}_A\right\|^2}\end{aligned} \tag{9}$$

$\mathbf{A}_i$ can be estimated through the vector colinear relationship in a color degeneration plane (see Fig. 1) by combining $\mathbf{I}(\mathbf{x})$ and $\mathbf{I}_p(\mathbf{y}_i)$ from (9). To briefly illustrate the calculation process of $\mathbf{A}_i$, $\mathbf{I}(\mathbf{x})$, $\mathbf{I}_p(\mathbf{y}_i)$, and $\mathbf{A}_i$ are transferred to the coordinate of $P(\mathbf{x})$ (see the right part of Fig. 4). Let $\mathbf{e}_A$ be the vertical axis of $P(\mathbf{x})$.

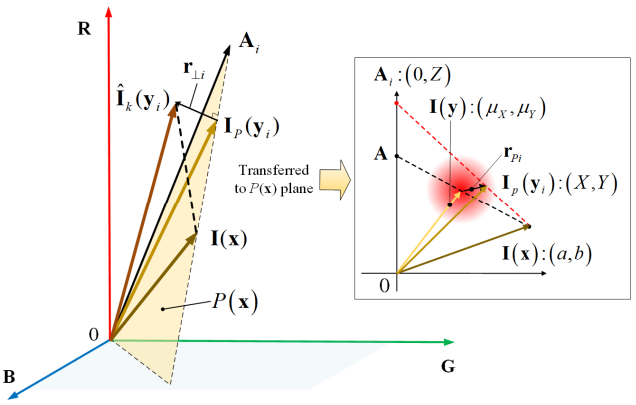

Fig. 4. Projection relationship of $\hat{\mathbf{I}}_k(\mathbf{y}_i)$, $\mathbf{I}(\mathbf{x})$, and $\mathbf{I}_p(\mathbf{y}_i)$.

$\mathbf{I}_P(\mathbf{y}_i)$ is the projection vector of $\hat{\mathbf{I}}_k(\mathbf{y}_i)$ on the $P(\mathbf{x})$, which also contains imaging and clustering error. Let $\mathbf{I}_P(\mathbf{y}_i)=\mathbf{I}(\mathbf{y})+\mathbf{r}_{Pi}$, where $\mathbf{I}(\mathbf{y})$ and $\mathbf{r}_{Pi}$ are in $P(\mathbf{x})$. $\mathbf{I}(\mathbf{y})$ represents the color vector without error and $\mathbf{r}_{Pi}$ is a random error vector induced by imaging and clustering. Assuming $\mathbf{r}_{Pi}$ to be a random variable which follows the normal distribution with zero mean and variance σ, the other error vector $\mathbf{I}_P(\mathbf{y}_i)$ become a random variable which follows the normal distribution with mean value $\mathbf{I}(\mathbf{y})$ and variance σ. Thus $\mathbf{A}_i$ becomes a random variable determined by $\mathbf{I}_p(\mathbf{y}_i)$ and $\mathbf{I}(\mathbf{x})$.

According to the right part of Fig. 4, the coordinate value of $\mathbf{I}(\mathbf{x})$ in the $P(\mathbf{x})$ is constant (a,b), where $b=\mathbf{I}(\mathbf{x})\cdot\mathbf{e}_A$ and $a=\sqrt{\|\mathbf{I}(\mathbf{x})\|^2-b^2}$. Assuming that the coordinate value of $\mathbf{I}(\mathbf{y})$ in the $P(\mathbf{x})$ is constant (μ_X,μ_Y), the coordinate value of $\mathbf{I}_p(\mathbf{y}_i)$ in the $P(\mathbf{x})$ is a random variable (X,Y), where $X\sim N(\mu_X,\sigma)$ and $Y\sim N(\mu_Y,\sigma)$. $Y=\mathbf{I}_p(\mathbf{y}_i)\cdot\mathbf{e}_A$ and $X=\sqrt{\|\mathbf{I}_p(\mathbf{y}_i)\|^2-Y^2}$. Then the coordinate value of $\mathbf{A}_i$ in the $P(\mathbf{x})$ is $(0,Z)$, which can be calculated as:

$$Z=b-\left(\frac{Y-b}{X-a}\right)\cdot a \tag{10}$$

According to random variables' function distribution, the probability density function (PDF) of Z in (10) can be deduced as:

$$f_Z(z)=\left[1-\frac{(z-A_{acc})\cdot z}{a^2+b^2+z^2}\right]\cdot\frac{1}{\sqrt{2\pi}\cdot\sigma_Z}\cdot e^{-\frac{(z-A_{acc})^2}{2\cdot\sigma_Z^2}} \tag{11}$$

where $A_{acc}=b-\frac{\mu_Y-b}{\mu_X-a}\cdot a$ and $\sigma_Z=\frac{\sqrt{a^2+b^2+z^2}}{a-\mu_X}\cdot\sigma$. A_{acc} represent the accurate module of atmospheric light determined by $\mathbf{I}(\mathbf{x})$ and $\mathbf{I}(\mathbf{y})$.

The (11) shows that the maximum value of PDF can be obtained when $z\to A_{acc}$. If the maximum value of PDF

statistics for $\|\mathbf{A}_i\|$ is located, the accurate module of atmospheric light A_{acc} can be obtained.

In order to locate the peak value of PDF reliably, the mean value of the top 5% count of $\|\mathbf{A}_i\|$ is treated as the peak value of PDF, and the corresponding horizontal coordinate value is treated as accurate module of atmospheric light.

The $\|\mathbf{A}_i\|$ can be directly calculated as:

$$\|\mathbf{A}_i\| = \frac{\left\|\mathbf{I}(\mathbf{x}) \times \left[\mathbf{I}_p(\mathbf{y}_i) - \mathbf{I}(\mathbf{x})\right]\right\|}{\left\|\mathbf{e}_A \times \left[\mathbf{I}_p(\mathbf{y}_i) - \mathbf{I}(\mathbf{x})\right]\right\|} \tag{12}$$

Then the PDF statistics for $\|\mathbf{A}_i\|$ can be carried out. As shown in Fig. 5, PDF statistics of $\|\mathbf{A}_i\|$ is shown as blue histogram. And the histogram is fitted with Eq. (11) (red curve) very well. According to the mean value location of the top 5% count of $\|\mathbf{A}_i\|$, the accurate module of atmospheric light is located as 329.

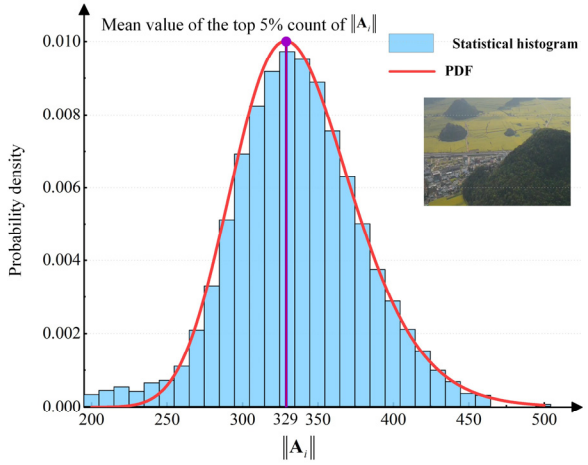

Fig. 5. Illustration of PDF statistics of $\|\mathbf{A}_i\|$ and fitting with Eq. (11)

In addition, the running time of the proposed atmospheric light estimation method can be accelerated through image sampling and by adjusting the number of the color clustering. Because the proposed method is dependent on the color clustering, a large number of repeated color vectors in the similar color class will influence the computational efficiency. Therefore, the original high-definition image with 1280×960 pixels can be sampled with equal intervals into an image of small 50×50 pixels. In this case, the number of the color clustering K on the 50×50 pixels influences the statistics of atmospheric light. If K is excessively large, the number of pixels for PDF statistics of atmospheric light's module is insufficient; If the K is extremely small, the color clustering is insufficient, and the estimation of atmospheric light's direction is easily influenced by the error of imaging and color clustering. According to the experimental verification, the K value is suggested to be 10.

IV. Experimental Results

In this section, the contrast analysis regarding the proposed method (Ours), DCP [21], Quad-tree [17], CAP [18], ATM [23], and Haze-lines [31] will be carried out.

The new large-scale benchmark RESIDE (Realistic Single Image Dehazing) [33] dataset, which contains subsets, such as Outdoor Training Set (OTS), Real-world Task-driven Testing Set (RTTS), Hybrid Subjective Testing Set (HSTS), was used for the experiments. OTS consists of 2061 real outdoor images from Beijing with scene depth data, which could be used for synthesizing various scenes under different atmospheric light and extinction coefficient [34]. RTTS consists of 4322 real outdoor digital images, including a variety of scenes and weather conditions. HSTS is a hybrid subjective test set with 20 clear images and synthesized haze images.

A. The Accuracy Analysis of Atmospheric Light Estimation with Labels

Based on the OTS dataset, a large number of synthetic scenes labeled with atmospheric light is generated. In order to set different value of atmospheric light, let each image contain different white light source (R=B=G) with grayscale values of 0-255 intervals (52 groups). Let atmospheric extinction coefficient changes (0 km^{-1}, 0.1 km^{-1}, 0.2 km^{-1}, 0.5 km^{-1}, 1.0 km^{-1}) to simulate different weather conditions [34], thus 535860 $(2061 \times 52 \times 5)$ outdoor images are generated.

The estimation results for the six methods at different setting value of atmospheric light are shown in Fig. 6. Compared to the other methods, the estimation results of the proposed method (marked in red) are closer to the setting value of atmospheric light.

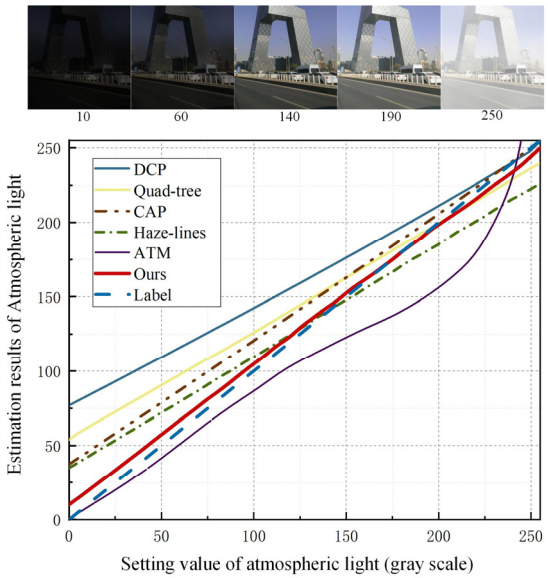

Fig. 6. Estimation results of atmospheric light for each method with given atmospheric light.

B. Image Dehazing Evaluation Based on the Atmospheric Light Estimation without Labels

In this section, the atmospheric light estimation is carried out based on the HSTS and RTTS datasets without labels. The atmospheric transmission estimation is based on the dark channel prior from Eq. (2). Then, by combining with atmospheric light estimation and atmospheric transmission estimation, the image dehazing can be achieved and evaluated.

Fig. 7 shows the image dehazing results and clear image from the HSTS dataset. The dehazing results of proposed method are closer to the clear image than other methods.

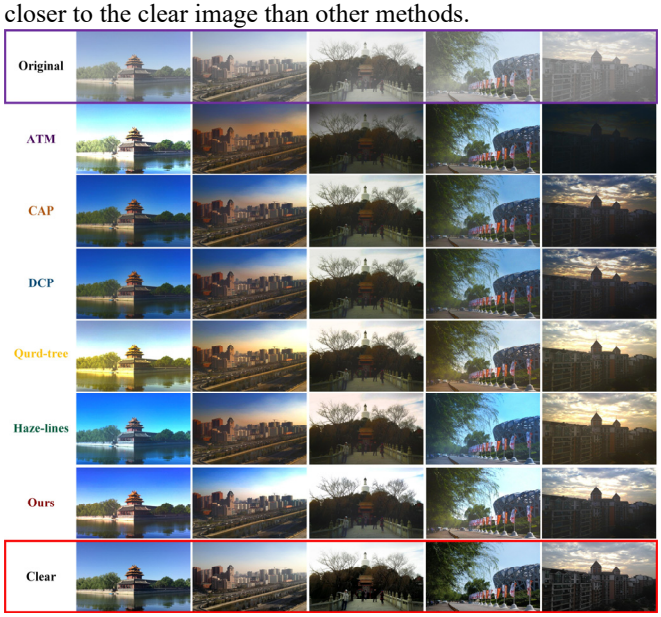

Fig. 7. Image dehazing results and clear image from the HSTS dataset.

To evaluate the quality of image dehazing, the Structural Similarity Index (SSIM) [35], Peak Signal to Noise Ratio (PSNR), Blind Reference less Image Spatial Quality Evaluator (BRISQUE) [36], and Naturalness Image Quality Evaluator (NIQE) [37] are adopted.

SSIM is used to evaluate the similarity of the dehazing image and clear image [35]. PSNR is used to evaluate the quality of the dehazing image and clear image $PSNR = 10\log_{10}\left(\frac{MAX^2}{MSE}\right)$ where MAX denotes max intensity of input image and MSE denotes mean square error. The higher score of SSIM and PSNR represents the higher image dehazing quality. BRISQUE is used for image enhancement, where the clear image is unknown. NIQE is computed based on the dehazing image. The higher score of SSIM and PSNR represents the higher image dehazing quality. The lower score of BRISQUE and NIQE represents the higher image dehazing quality.

Fig. 8 shows the quality evaluations with SSIM, PSNR, BRISQUE, and NIQE based on the HSTS dataset. The proposed method for image dehazing reaches the best results under SSIM, PSNR and BRISQUE and the second best under NIQE.

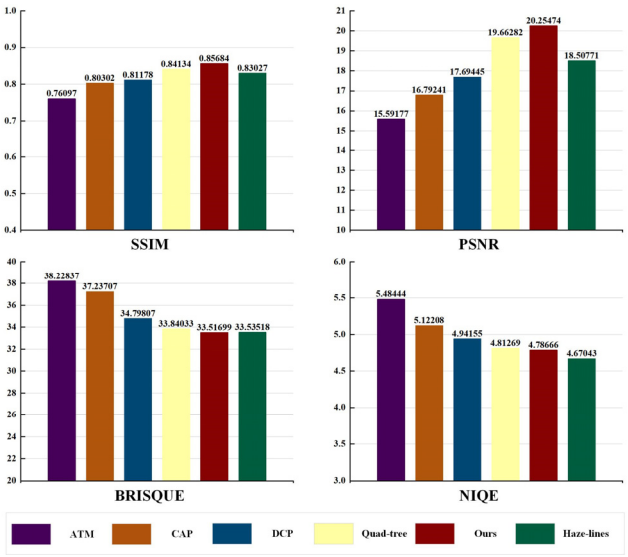

Fig. 8. Quality evaluation for image dehazing

Based on the RTTS dataset, the dehazing results under three scenarios of darkness, traffic, and dust are shown in Fig. 9. Moreover, the proposed method performs better in dark scenes than other methods.

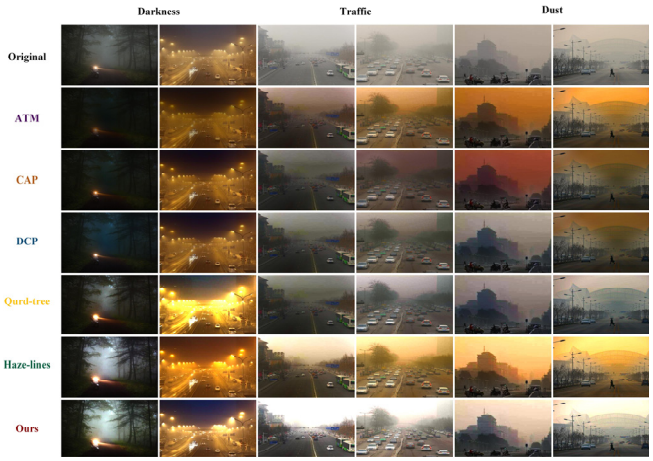

Fig. 9. Example of dark, traffic, and dusty scene images

C. Running Time Comparisons

The running time of different methods are compared at different image sizes. The computer configuration is as follows. CPU: AMD Ryzen7 4800H, RAM: 16G. As shown in Fig. 10, because the proposed method is operated with sampled small image (50×50), the running time of the proposed method remains a short constant even if the image resolution increases above 1280×960.

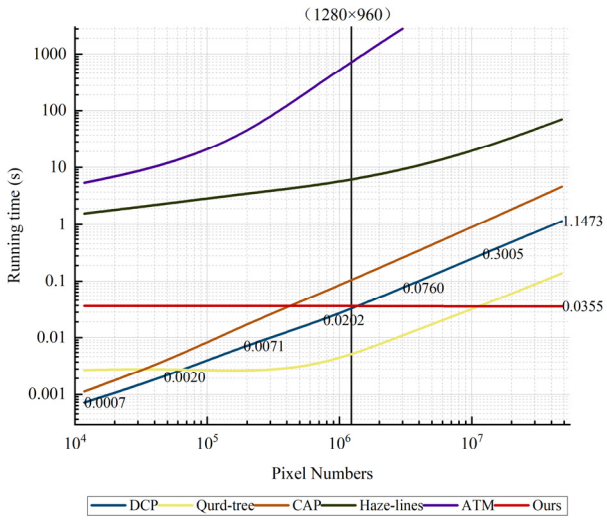

Fig. 10. Running time of different methods with different pixel numbers

V. Conclusion

This study reveals a vector orthogonality in the classical atmospheric color degradation model for the first time, that is, it is demonstrated that the atmospheric light vector is orthogonal to the normal vectors of color degradation plane. By Combining the vector orthogonality and the color clustering, a novel estimation method for atmospheric light vector' direction is proposed by solving the least square solution which implies that the atmospheric light vector' direction is orthogonal to all the normal vectors of color degradation planes. Moreover, a novel estimation method for atmospheric light vector' module is proposed by PDF statistics calculated by randomly chosen color vectors in a similar color class. It can be observed that the proposed method can accurately estimate the atmospheric light and improve the quality of image dehazing with a short constant processing time even if the image resolution is increasing. The study provides an efficient way to estimate the atmospheric light for high-definition image or video dehazing applications, such as traffic surveillance, environmental monitoring, and aerial photography.

Further theoretical researches regarding the optimization of image sampling and color clustering could be carried out. The best combination of the proposed atmospheric light estimation method and atmospheric transmission estimation method could be carried out. In addition, the feasibility of using the proposed method for water background light estimation is required to be investigated.

References

[1] R. T. Tan, "Visibility in bad weather from a single image" IEEE Comput. Soc. Conference on Computer Vision and Pattern Recognition (CVPR 2008), pp. 24-26 Anchorage, Alaska, USA: IEEE, 2008.
[2] E. J. Mccartney and F. F. Hall, "Optics of the atmosphere: Scattering by molecules and particles," *Phys. Today*, vol. 30, no. 5, pp. 76–77, 1977 [DOI: 10.1063/1.3037551].
[3] S. G. Narasimhan and S. K. Nayar, "Vision and the atmosphere," *Int. J. Comput. Vis.*, vol. 48, no. 3, pp. 233-254, 2002 [DOI: 10.1023/A:1016328200723].
[4] S. G. Narasimhan and S. K. Nayar, "Contrast restoration of weather degraded images," *IEEE Trans. Pattern Anal. Mach. Intell.*, vol. 25, no. 6, pp. 713-724, 2003 [DOI: 10.1109/TPAMI.2003.1201821].
[5] S. G. Narasimhan and S. K. Nayar, "Chromatic framework for vision in bad weather". IEEE Comput. Soc. Conference on Computer Vision & Pattern Recognition. IEEE, 2000.
[6] S. G. Narasimhan and S. K. Nayar, *Interactive (De) Weathering of an Image Using Physical Models*, 2015.
[7] Bolun Cai *et al.*, "Dehazenet: An ensd-to-end system for single image haze removal," *IEEE Trans. Image Process.*, vol. 25, no. 11, pp. 5187-5198, 2016 [DOI: 10.1109/TIP.2016.2598681].
[8] B. Li *et al.*, "AOD-net: All-in-one dehazing network" IEEE International Conference on Computer Vision (ICCV), vol. 2017. IEEE, 2017.
[9] D. Yang and J. Sun, "Proximal dehaze-net: A prior learning-based deep network for single image dehazing". Eur. Conference on Computer Vision. Cham: Springer, 2018.
[10] Y. Qu *et al.*, *Enhanced Pix2pix Dehazing Network*, vol. 2019. IEEE/CVF Conference on Computer Vision and Pattern Recognition (CVPR). IEEE, 2019.
[11] X. Qin *et al.*, "FFA-net: Feature fusion attention network for single image dehazing". National Conference on Artificial Intelligence. Association for the Advancement of Artificial Intelligence (AAAI), 2020.
[12] Q. Deng *et al.*, "HardGAN: A haze-aware representation distillation GAN for single image dehazing". Eur. Conference on Computer Vision. Cham: Springer, 2020.
[13] X. Liu *et al.*, "Mlfcgan: Multi-level feature fusion based conditional gan for underwater image color correction," *IEEE Geosci. Remote Sens. Lett.*, vol. 17, no. 9, 1488–1492, 2020 [DOI: 10.1109/LGRS.2019.2950056].
[14] H. Wu, et al., *Contrastive Learning for Compact Single Image Dehazing*, 2021.
[15] X. Zhang, et al., *Learning to Restore Hazy Video: A New Real-World Dataset and A New Method. Computer Vision and Pattern Recognition*. IEEE, 2021.
[16] Raanan and Fattal, "Dehazing using color-lines," *ACM Trans. Graph. (TOG)*, vol. 34, no. 1, 2014.
[17] J. H. Kim *et al.*, "Optimized contrast enhancement for real-time image and video dehazing," *J. Vis. Commun. Image Represent.*, vol. 24, no. 3, pp. 410–425, 2013 [DOI: 10.1016/j.jvcir.2013.02.004].
[18] Q. Zhu *et al.*, "A fast single image haze removal algorithm using color attenuation prior," *IEEE Trans. Image Process.*, vol. 24, no. 11, pp. 3522-3533, 2015 [DOI: 10.1109/TIP.2015.2446191].
[19] D. Berman *et al.*, "Non-local image dehazing" IEEE Conference on Computer Vision and Pattern Recognition (CVPR), vol. 2016. IEEE, 2016.
[20] J. Liu *et al.*, *Rank-One Prior: Toward Real-Time Scene Recovery*, 2021.
[21] K. He and S. Jian, "Fellow, IEEE, & Tang, X," *IEEE Transactions on Pattern Analysis & Machine Intelligence*, vol. 33, no. 12, pp. 2341-2353, 2011. Single image haze removal using dark channel prior.
[22] J. P. Tarel and N. Hautière, "Fast visibility restoration from a single color or gray level image". IEEE International Conference on Computer Vision. IEEE, 2010.
[23] M. Sulami *et al.*, "Automatic recovery of the atmospheric light in hazy images". IEEE International Conference on Computational Photography. IEEE, 2014.
[24] R. Fattal, "Single image dehazing," *ACM Trans. Graph.*, vol. 27, no. 3, 1–9, 2008 [DOI: 10.1145/1360612.1360671].
[25] J. G. Jiang *et al.*, "Improved algorithm on image haze removal using dark channel prior," *J. Circuits Syst.*, vol. 16, no. 2, pp. 7-12, 2011.
[26] M. K. Das *et al.*, "Image dehazing using improved dark channel prior and relativity of Gaussian," *Procedia Comput. Sci.*, vol. 165, pp. 442-448, 2019 [DOI: 10.1016/j.procs.2020.01.004].
[27] Sahu, G. , Seal, A. , Krejcar, O. , & Yazidi, A. . (2020), "Single image dehazing using a new color channel," *J. Vis. Commun. Image Represent.*, vol. 74, no. 5, p. 103008.
[28] L. Zhang *et al.*, "Single image dehazing based on bright channel prior model and saliency analysis strategy," *IET Image Process.*
[29] Lin, Z. , and X. Wang., "Dehazing for Image and Video Using Guided Filter" Open Journal of Applied Sciences, 2012.
[30] J. Wang *et al.*, "Single image dehazing based on the physical model and msrcr algorithm," *IEEE Trans. Circuits Syst. For Video Technol.*, vol. 28, no. 9, 2190–2199, 2017 [DOI: 10.1109/TCSVT.2017.2728822].
[31] D. Berman *et al.*, "Air-light estimation using haze-lines" IEEE International Conference on Computational Photography (ICCP), vol. 2017. IEEE, 2017.

[32] A. Golts, D. Freedman, E. Michael. (2019). Unsupervised single image dehazing using dark channel prior loss. IEEE Trans Image Proc., PP(99), 1-1.
[33] B. Li, W. Ren, D. Fu, D. Tao, D. Feng, and W. Zeng, et al. "Benchmarking single image dehazing and beyond.
[34] F. Liu, C. Shen, G. Lin, and I. Reid, "Learning depth from single monocular images using deep convolutional neural fields," *IEEE Trans. Pattern Anal. Mach. Intell.*, vol 38, no.10, pp. 2024-2039, 2015.
[35] W. Zhou, A. C. Bovik, H. R. Sheikh, and E. P. Simoncelli, "Image quality assessment: from error visibility to structural similarity," *IEEE Trans. Image Process.*, vol. 13, no. 4, pp. 600-612, Apr 2004, doi: 10.1109/TIP.2003.819861.
[36] A. Mittal, A. K. Moorthy, and A. C. Bovik, "No-reference image quality assessment in the spatial domain," *IEEE Trans Image Process A*, vol. 21, no. 12, pp. 4695, Aug 2012, doi: 10.1109/TIP.2012.2214050.
[37] A. Mittal, Fellow, IEEE, R. Soundararajan, and A.C. Bovik, "Making a 'completely blind' image quality analyzer. *IEEE Signal Process Lett.*," vol. 20, no. 3, pp. 209-212,Nov 2013, doi: 10.1109/LSP.2012.2227726.

LINGZHAO KONG received his B.E. degree from the North University of China, Taiyuan, China in 2020. He is currently working toward a master's degree at the School of Aeronautics and Astronautics, University of Electronic Science and Technology of China, Chengdu 611731, China. His current research interests include free-space optical communications, image enhancement.

DAGANG JIANG (Member, IEEE) received the B.S. and M.S. degrees from the Beijing University of Aeronautics and Astronautics, in 2004 and 2007, respectively, and the Ph.D. degree in optics from the University of Electronic Science and Technology of China, in 2014. He is currently an Associate Professor with the University of Electronic Science and Technology of China and the Associate Director of the Aircraft Swarm Intelligent Sensing and Cooperative Control Key Laboratory of Sichuan Province. His current research interests include free space optical communication and laser atmospheric propagation.

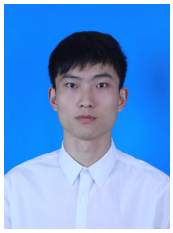

XIN LIU (Student Member, IEEE) received the B.A.Sc. degree from the Changchun University of Science and Technology, Changchun, China, in 2017. He is currently pursuing the Ph.D. degree with the School of Engineering, University of Electronic Science and Technology of China, Chengdu, China. His current research interests include free-space optical communications, atmospheric optical communication, and propagation of laser beams in atmosphere turbulence.

YU ZHANG received her B.E. degree from the Southwest Minzu University, Chengdu, China in 2020. She is currently working toward a master's degree at the School of Aeronautics and Astronautics, University of Electronic Science and Technology of China, Chengdu 611731, China. Her main research direction is image processing.